Journal of Molecular Liquids 360 (2022) 119492

Contents lists available at ScienceDirect

Journal of Molecular Liquids

journal homepage: www.elsevier.com/locate/molliq

# Phenol-cyclohexanol eutectic mixtures: Phase diagram and microscopic structure by experimental and computational studies ☆

Simone Di Muzio [a,b], Annalisa Paolone [b], Olga Russina [c], Fabio Ramondo [c,*]

[a] Department of Physical and Chemical Sciences, University of L'Aquila, Via Vetoio, I-67100 L' Aquila, Italy
[b] Istituto dei Sistemi Complessi-Consiglio Nazionale delle Ricerche-ISC-CNR U.O.S. Sapienza, P.le A. Moro 5, 00185 Rome, Italy
[c] Department of Chemistry, University of Rome 'La Sapienza', P.le Aldo Moro 5, I-00185 Rome, Italy

ARTICLE INFO

*Article history:*
Received 28 March 2022
Revised 24 May 2022
Accepted 26 May 2022
Available online 30 May 2022

*2010 MSC:*
00-01
99-00

*Keywords:*
Deep eutectic solvent
Hydrogen bond
Molecular dynamic
DSC
X-ray diffraction
DFT
FT-IR

ABSTRACT

Non ionic deep eutectic solvents (type V) have been recently proposed as innovative and alternative solvents. Prepared by mixing the starting components, their mixtures show strong deviations from thermodynamic ideality. An example of deep eutectic solvent is the 1:1 thymol-menthol mixture: deviations from ideality are originated from the strength of the hydrogen bond between different components. With the aim to investigate the role of hydrogen bonding in the non-ideality of mixtures of phenolic and alcoholic compounds, we studied the phase diagram and the structural properties of cyclohexanol and phenol mixtures coupling experimental and computational techniques. The phase diagram was measured by differential scanning calorimetry (DSC) providing a lowest melting point at about ,-35°C. The microscopic structure of eutectic composition was characterized by infrared spectroscopy (FT-IR), DFT and classical molecular dynamic simulations. The X-ray pattern was compared with MD results with the aim to describe the intermolecular interactions between phenol and cyclohexanol. The deviations from ideal mixing seem to be smaller than those observed for the 1:1 thymol-menthol mixture. The nature of intermolecular interactions in the phenol-cyclohexanol system has been compared with that of the thymol-menthol system by quantum chemistry calculations. In both the systems heteroassociation is energetically preferred to homoassociation because hydrogen bonding is stronger between different components, however van der Waals contributions involving alkyl groups can play an additional and significant role in the intermolecular association of the thymol-menthol system.



## 1. Introduction

As a promising alternative to classical solvents, eutectic solvents (ESs) have received an increased interest in the past two decades. They show most of the properties of the ionic liquids (ILs), including low volatility and high solvating and extracting properties, with the advantage that they are usually less toxic variants of the room temperature ionic liquids. As ILs, ESs exhibit a wide number of tunable physicochemical properties [1–4] that allow their utilization in a growing number of fields, including extraction, (bio) synthesis, catalysis, electrochemistry, and carbon dioxide capture [5–9]. The majority of ESs are easily prepared by mixing biodegradable starting materials, like organic or inorganic salts, with organic acids or organic neutral molecules. Deep eutectic solvents (DESs) are ESs whose properties deviate significantly from thermodynamic ideality: these mixtures show melting points much lower than their starting components and the term DES was introduced to highlight this property [10]. The strong intermolecular interactions formed mixing of a H-bond donor (HBD) with a H-bond acceptor (HBA) or with a molecular ionic species favor specific spatial correlations between the DES constituents and cause noticeable non-ideal mixing effects that could explain the exceptional lowering of the melting point of certain DESs. Some structural studies on choline chloride [Ch][Cl] mixed with HBDs, like urea [11,12] or carboxylic acids [13,14], revealed that the main driving force for melting point depression is the formation of hydrogen bonding between the HBD and the anion.

However the hydrophilicity of most DESs limits their practical application to only polar compounds, which is a major drawback of these solvents. Hydrophobic DESs have emerged as an alternative media capable of extracting non-polar organic and inorganic molecules from aqueous solutions [15]. DESs with hydrophobic properties were obtained by selecting quaternary ammonium salts and acids or alcohols having long side alkyl chains [16]. Their

☆ Fully documented templates are available in the elsarticle package on CTAN.

* Corresponding author.
*E-mail address:* fabio.ramondo@uniroma1.it (F. Ramondo).

https://doi.org/10.1016/j.molliq.2022.119492
0167-7322/

extraction capacity of volatile fatty acids [17] from aqueous solution and their solvent properties of carbon dioxide [18] can be be modulated by the length of the alkyl chain of the cation. Another class of hydrophobic DESs is composed of only nonionic molecular HBAs and HBDs, and the first non-ionic deep eutectic liquid was identified in 1958 by mixing urea and acetamide [19]. Mixtures of N-alkyl derivaties of acetamide and urea have been identified as deep eutectic systems for the non-ideal mixing of their component [20] and have been employed in the polymer synthesis [21]. Notwithstanding these mixtures lack ionic contribution, they still exhibit DES melting point characteristics and it is thought that hydrogen bonding is responsible for the lowering of melting point [22]. More recently non ionic eutectic mixtures of natural compounds, as terpenes and carboxylic acids, has been proposed and widely used in the pharmaceutical field [23–25]. The eutectic system composed by thymol and menthol, proposed by Coutinho and coworkers [26] and classified as Type V DESs, is particularly interesting for the complex intermolecular interactions between components. Although thymol and menthol have similar structures and they can form hydrogen bonding both like pure components as well as like mixed components, their mixtures show strong negative deviations from the thermodynamic ideal mixing [27]. The non ideality of this system has been attributed to the feature of the hydrogen bond between thymol and menthol that is stronger than that between thymol-thymol and menthol-menthol in the pure substances [26,27]. This consideration has been supported by experimental $^{1}H_{1}$ NMR and Raman spectroscopy, X-ray scattering diffraction [27] and molecular dynamic simulations [27,28]. The severe negative deviations from ideality of this mixtures derive therefore from the acidity difference between phenolic and hydroxyl groups. As suggested in previous studies [26], these deviations do not seem to be specific of the binary thymol-menthol systems but are expected in all the systems where a compound with the hydroxyl group connected to a benzene ring is mixed with a second compound where the hydroxyl group is bonded to an alkyl chain. To further investigate the role of phenolic hydrogen bond in the formation of non ionic DESs we investigated in the present study the phenol-cyclohexanol mixture, the simpler version of the thymol-menthol system. Melting temperature at different molar ratios has been measured by Differential Scanning Calorimetry (DSC) to study the phase diagram of the system and to determine the eutectic composition. Intermolecular interactions between the components and their distribution in the mixture has been investigated through a combination of infrared spectroscopy, X-ray diffraction and theoretical investigations by quantum mechanical (QM) methods and molecular dynamics (MD) simulations.

## 2. Materials and procedures

### 2.1. Materials and sample preparation

Phenol, PhOH, (98%) and cyclohexanol, CycOH, (99%) were purchased from Merck and the purity of each sample was confirmed by $^{1}H_{1}$ NMR and $^{13}C_{13}$ NMR spectroscopy, using a Bruker Avance III spectrometer operating at 400 MHz and 100.6 MHz, respectively. PhOH-CycOH binary mixtures at different molar ratios were prepared and the liquid, formed at 80°C, was than dried *in vacuo* at 70°C overnight to obtain the final product. All the mixtures were then stored in sealed vials before measurements.

#### 2.1.1. Differential scanning calorimetry

DSC curves were acquired using a Mettler Toledo DSC 3 Star System instrument. Cyclohexanol and phenol were heated from room temperature (RT) up to 60°C, kept in isothermal conditions for ten minutes, cooled at -90°C and kept at this temperature for ten minutes; finally, the temperature was increased to 60°C. On the other hand, all mixtures were cooled from RT to -90°C, kept in isothermal condition for ten minutes and heated up to 60°C. The scanning rates applied were $\Delta T/\Delta t$ = 5 K/min and $\Delta T/\Delta t$ = 0.6 K/min, under an Ar gas flow of 50 ml/min.

#### 2.1.2. X-ray scattering

Wide Angle X-ray Scattering (WAXS) experiments were carried out by means of a Bruker D8 Advance diffractometer located at CNIS LAB Sapienza. The instrument operates with a Mo Kα X-ray tube (λ = 0.7107 Å) and Göbel mirrors collimation optics. The data have been collected in transmission mode in 2θ angle range from 2.75° up to 142° with a step of 0.25°. The sample was inserted in a quartz capillary (2 mm radius) and sealed. The collected data have been corrected for the background and sample absorption. Static structure factor I(q) has been obtained by subtraction of atomic scattering and inelastic scattering contribution.

#### 2.1.3. Infrared spectrocopy

Infrared absorbance spectra were acquired by means of an Agilent Cary 660 spectrometer, equipped with a KBr beamsplitter and DTGS detector. The phenol spectrum was measured dissolving the solid in KBr salt, in a proportion of about 1:100. Cyclohexanol and its mixtures with phenol, that are liquids at room temperature, were placed between the optical diamond windows of a vacuum tight cell, separated by a spacer with a thickness of 10 μm. All spectra were measured at room temperature with a resolution of 1 $cm^{-1}$.

#### 2.1.4. Computational details

The structure of the liquid mixtures has been investigated following two theoretical approaches. The intermolecular interactions between different components have been initially studied by *ab initio* methods. Two cyclic tetramers consisting of phenol (Figs. 1a and 1b and cyclohexanol (Fig. 1c) molecules have been investigated to evaluate hydrogen bonding in each pure component. A third tetramer consisting of two phenol and two cyclohexanol molecules (Fig. 1d) has been proposed to evaluate hydrogen bonding between different components, as expected for our mixtures. Quantum-mechanical (QM) calculations of each tetramer were performed by the Gaussian 09 package [29]. Equilibrium geometry and IR spectra were obtained using density functional theory (DFT) methods with the Minnesota meta hybrid CGA M062X [30] exchange and correlation functional and employing the 6-311G** basis set. Vibrational modes of each system have been assigned on the basis of the analysis of the normal modes. The good reliability of such a functional in describing energetic and structural aspects of several liquids has been discussed in earlier reports [31]. Analogous oligomers have been considered for the thymol-menthol system by studying the molecular geometries obtained by M062X/6-311G** calculations for the tetramers of menthol and thymol and for a tetramer formed by two thymol and two menthol molecules within the same symmetry adopted for the phenol and cyclohexanol clusters. Their structure is reported in Fig. S1.

To more deeply analyze the topological and energetic characteristics of the hydrogen bond in each molecular complex Atoms in Molecules (AIM) studies were performed employing the software AIMAll (Version 19.10.12) [32]. Non-Covalent Interaction analysis (NCI)[33] was also developed for the optimized clusters using the MultiWFN procedure[33].

MD simulations were performed in order to conduct a global investigation on the structure of liquid. We simulated the mixture at the eutectic composition (molar fraction of cyclohexanol equal

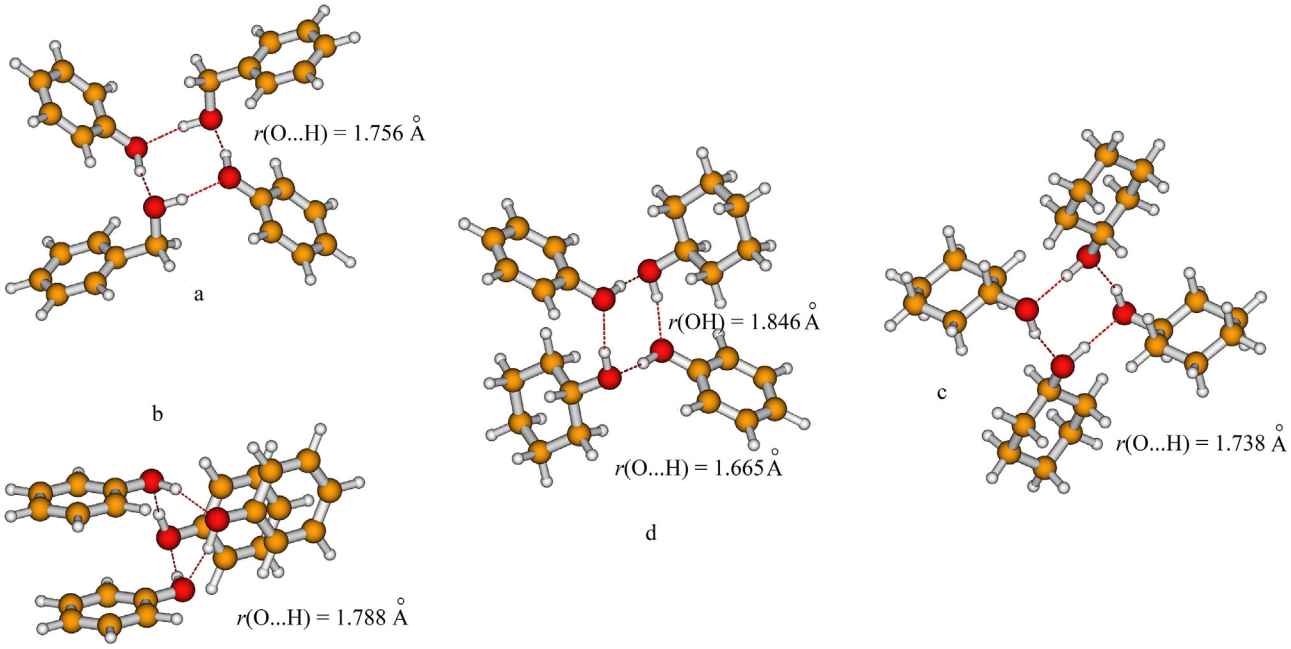


**Fig. 1.** Tetramers of phenol, (a and b, $S_4$ symmetry), cyclohexanol (c, $S_4$ symmetry) and phenol-cyclohexanol (d, $C_2$ symmetry).

to 0,85) using the two-body Generalized Amber Force Field (GAFF) [34]. Topology and input files were written using Amber software [35] and then converted to Gromacs format. Partial atomic charges were computed using Gaussian09 [29] at level HF/6-31G*: Restrained Electrostatic Potential (RESP, [36]) was chosen as algorithm and charges calculations were computed on isolated species. Electrostatic interactions were considered by Particle Mesh Ewald (PME) under periodic boundary conditions (PBC). All bonds with hydrogen bond were studied using the Linear Constrain Solver (LINCS) algorithm [37]. Parallelization were conducted using the domain decomposition algorithm and Message Passing Interface paradigm (MPI). The cut off radii of van der Waals and direct-space Ewald interactions were imposed at 1 nm. The randomic starting configuration were obtained putting 850 molecules of cyclohexanol and 150 of phenol into a box with the initial side of 80Å, using PACKMOL [38] software. Energy minimization has been carried out during $10^7$ iterations. The starting box was simulated for 2250 ps in NVE ensemble and for 40 ns in NPT ensemble at 400 K monitoring the pressure with Berendsen barostat and the temperature with Nos-Hoover thermostat. The simulations at 400 K have been conducted in order to decrease the viscosity of the liquid during the initial phases of our simulation. At this point we have decreased the value of temperature at 323 K. The density of liquids were calibrated by a long NPT simulation (20 ns). A very long NVT simulations (50 ns) have been performed with the aim to equilibrate the system. Structure factors I(q) have been calculated from the molecular dynamics trajectories using the Travis software [39,40]. Theoretical I(q) has been then multiplied by $q$ to obtain a theoretical qI(q) function comparable with the experimental one.

## 3. Results and discussion

### 3.1. DSC

The eutectic point of the PhOH-CycOH binary system can be estimated by the following equation[41]

$$ln(a_i) = \frac{\Delta H_m}{R}\left(\frac{1}{T_m} - \frac{1}{T}\right) \quad (1)$$

where $a_i$ is the activity of the component i, $T_m$ and $\Delta H_m$ are the melting temperature and enthalpy of the pure compound, respectively, and $R$ is the universal gas constant, by assuming an ideal liquid mixture ($a_i = x_i$). In the previous equation we consider negligible the difference between the molar heat capacity of the component *i* in the liquid and solid phase. Within the validity of this equation, we can predict the solid-liquid equilibrium (SLE) phase diagram for an ideal mixture (Fig. S2). The eutectic composition is expected at molar ratios of cyclohexanol, here after indicated as ($x_c$), close to 0.8. Starting from this consideration, the phase diagram of the PhOH-CycOH system has been studied by differential scanning calorimetry (DSC) preparing mixtures of composition not too far from to this value. In Fig. 2 we reported the DSC curves of the pure cyclohexanol, pure phenol along with ten their mixtures.

The DSC curve of pure cyclohexanol shows three thermal processes: the most important is centred at 25.6°C and corresponds to the melting point. Cyclohexanol has a polymorphic structure and the accurate description of the polymorphism has been investigated in previous works [42–44]. In agreement with the previous literature [42–44], the endothermic peaks between -50°C and -20°C can be attributed to solid-solid phase transitions between polymorphs. The DSC curve of pure phenol is much simpler, as it displays only an endothermic peak around 45°C, corresponding to the melting.

An eutectic composition is an homogeneous phase that melts at a single temperature, according to the thermodynamic definition. Moving apart from the eutectic composition, the other mixtures should show two melting peaks: one close to that of the eutectic and the other related to the phase containing an excess of one of the two constituents. Indeed, in our system we observe two melting processes for the non-eutectic compositions with $x_c \neq 0.85$.

In the case of $x_c$ = 0.98 we observed two endergonic transitions: the first, at 17°C, is attributed to the melting of a phase rich in cyclohexanol and the other one, at -28°C, is the melting of a quasi-eutectic phase. A cold crystallization peak is present around -65°C. The difference between the two melting temperatures decreases as the composition approaches the eutectic. In fact, in the case of $x_c$ = 0.95 the first endothermic transition is at 6°C and

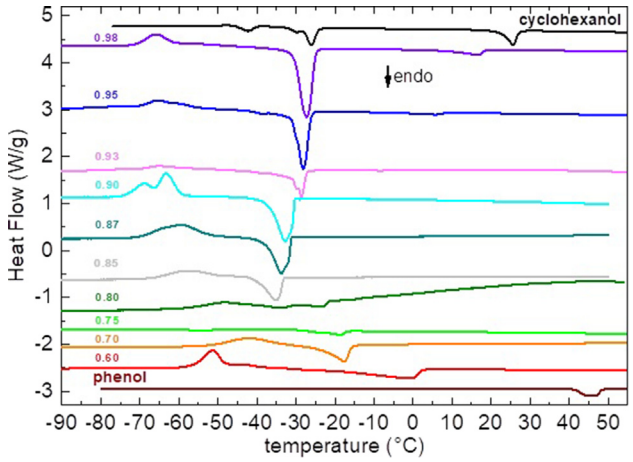


**Fig. 2.** DSC curves for cyclohexanol and phenol pure components and for their mixtures at different compositions.

the second at -28°C. The mixture $x_c$ = 0.93 clearly shows the lower temperature peak (T=-29°C), while the second peak centred around -9°C has an extremely low integral. Turning to the less concentrated compositions ($x_c$ 0.75) the DSC curves appear slightly different, as only one endothermic peak is clearly visible. All melting processes are anticipated by a cold crystallization below -30°C. For $x_c$ = 0.70 and $x_c$ = 0.60 the melting peaks are at -18°C and -0.7°C, respectively. The intermediate compositions (0.80 $x_c \leqslant$0.93), when measured at the same temperature scanning rate used for the previously reported mixtures, do not show clear phase transitions (results not shown). For $x_c \geqslant$0.95 and $x_c \leqslant$0.75 it was already observed that the samples do not undergo any crystallization on cooling, but more likely they present cold crystallizations on heating. This fact suggests that the crystallization of samples is slow and can be suppressed or retarded at high temperature rates. Therefore, for samples with 0.80 $\leqslant x_c \leqslant$0.93, DSC measurements were repeated with a much slower temperature scanning rate ($\Delta T/\Delta t$ = 0.6 K/min), 9 times slower than the previous one. As reported in Fig. 2, all these samples present a cold crystallization (with maxima at −65.2,-63.2, −59.3, −57.7, −48.0 °C for $x_c$ = 0.93, 0.90, 0.87, 0.85, 0.80, respectively) and a melting process with minima at −28.5, −32.7, −33.7, −35.0, −34.1 °C for $x_c$ = 0.93, 0.90, 0.87, 0.85, 0.80, respectively. Apart for $x_c$ = 0.85 the melting peak seems to be composed of two different components. The lowest melting temperature is found at the composition $x_c$ = 0.85: this mixture shows a single peak centred at −35 °C. Therefore, we assume that the eutectic composition is close to $x_c$ = 0.85.

By examining the values of the melting temperatures measured by our DSC experiment and summarized in Table S1 we observe that they are quite close to those derived from the SLE phase diagram predicted by assuming an ideal liquid phase (activity coefficient equal to one) (Fig. S2). The experimental SLE phase diagram gives therefore an eutectic point not very far from that expected from a ideal mixture. This result suggests that the phenol-cyclohexanol system presents a quasi-ideal behavior with small deviations from ideality. As matter of fact, negative deviations from ideality are expected for the binary PhOH-CycOH binary system [45,46] and when values of activity coefficients derived from SLE measurements [46] are introduced in the Eq. (1), a small depression of the eutectic temperature (about 10°C) is predicted (see Fig. S1). This behavior seems therefore to be quite different from the thymol-menthol binary system where a very deep depression (60 °C) of the melting temperature with respect to ideality has been observed and predicted [26,27].

### 3.2. Interaction models by quantum chemistry

With the aim of understanding the features of our eutectic mixtures and investigate the nature of the interactions between their components, we studied by theoretical methods a series of complexes where PhOH and CycOH interact each other by different geometries. We started to consider the tetramers reported in Fig. 1 by analyzing their structures obtained by quantum mechanical calculations at the M062X/6-311G** level. In the phenol crystal, the molecules are connected via OH···O hydrogen bonds into endless helical chains [47] and simple simulations of the crystal field unequivocally showed that hydrogen bond formation causes outstanding changes in the molecular geometry [48]. Therefore any molecular model proposed to describe the properties of pure phenol should start by molecules connected each other by hydrogen bonds and the cyclic tetramers reproduced in Figs. 1a and 1b are reasonable molecular structures where each OH group is involved in OH···O hydrogen bond and acts both like HB donor and like HB acceptor. Starting from this cyclic arrangement of phenol molecules, two geometries, both of $S_4$ symmetry, were found as stable structures: Fig. 1a shows a cyclic tetramer where molecules are connected only via OH...O hydrogen bonds whereas Fig. 1b shows that the benzene rings are oriented to form additional π-π stacking interactions. Such a favorable alignment of the benzene rings gives a higher stability (27 kJ/mol) with respect to the 1a tetramer, although the OH···O distances are longer (1.788 Å) than those of the 1a tetramer (1.756 Å).

As already observed, surprisingly complex polymorphic behavior has been observed for cyclohexanol [42,43,49]. This simple molecule exhibits rich polymorphism that may be attributed to its conformational flexibility and capacity to form hydrogen bonds. The phase diagram of CycOH has been studied following several experiments [42,43,49,50,44]: it has a melting point of 298 K and crystallizes in a plastic, orientationally disordered phase (phase I) which includes both axial and equatorial orientational configurations of the hydroxyl group and orientational disorder of the cyclohexyl ring [50]. At 265 K CycOH crystallizes in a phase II where molecules are arranged in a hydrogen-bonded tetrameric ring structure. Due to its conformationally mobility it is quite hard to propose a simple model to simulate the complexity of hydrogen bonding in liquid and phase I states. The cyclic tetramer here presented (Fig. 1c) is probably more suitable to describe molecules involved in hydrogen bonding networks as occurs in the crystal phases. However this model offers the advantage to describe four CycOH molecules that, acting as HB acceptors as well HB donors, form four equivalent hydrogen bonds and allows an easy comparison with hydrogen bonding of the PhOH tetramer. Each cyclohexanol is assumed in chair conformation with the hydroxyl group in an equatorial orientation.

The mixing of cyclohexanol and phenol allows interactions between different components. In order to evaluate hydrogen bonding between PhOH and CycOH we studied the tetramer of Fig.1d with $C_2$ symmetry, where two phenol and two cyclohexanol molecules are alternate and cyclically arranged to form two types of interactions: hydrogen of phenol interacts with oxygen of cyclohexanol and simultaneously hydrogen of cyclohexanol interacts with oxygen of phenol.

The O···H intermolecular distances calculated for the homotetramers (see Fig. 1) suggest that cyclohexanol promotes a more efficient hydrogen bond. Whereas PhOH is an excellent HB donor but poor HB acceptor, CycOH can act both as HB donor and acceptor, as a classical alcohol, and it is expected to form stronger hydrogen bonds. In the mixed tetramer (Fig. 1d) the HB donor property of PhOH coupled with the optimal HB acceptor property of CycOH gives the formation of the shortest intermolecular O···H distances

(1.665 Å). An analysis of a wide number of crystal structures showed in fact that heteromeric HB between phenols and alcohols occurs more often than homomeric HB [51].

AIM analysis provides additional information on the nature of the intermolecular interactions and with this aim some topological criteria were proposed by Koch and Popelier [52]. Among them, we considered here the existence of bond critical points ($r_c$) on the bond path between the hydrogen and the oxygen acceptor and the values of electron density and Laplacian of electron density at the bond critical point, $\rho(r_c)$ and $\nabla^2(r_c)$, respectively. Their values are reported in Table 1 and, consistently with the O···H distances, they indicate that cyclohexanol forms hydrogen bonds more stable than those formed by phenol. Rozas et al. [53] have classified hydrogen bonds on the basis of $\nabla^2(r_c)$ and total electron energy density $H(r_c)$ defined as sum of kinetic and potential electron densities at the bond critical point. The negative values of $H(r_c)$ values reveal that both the hydrogen bonds in phenol and cyclohexanol can be classified as strong and a small preference is expected for cyclohexanol, in agreement with the values of the O···H distances. In the heterotetramer PhOH and CycOH are linked via stronger hydrogen bonds, as suggested by the AIM results reported in Table 1 and in agreement with the O···H distances. All the computational results here reported indicate therefore the preferential nature of the PhOH-CycOH HB with respect to the PhOH-PhOH and CycOH-CycOH HB interactions.

The strength of the interactions between molecules in each cluster has been estimated by calculating the interaction energy (ΔE) as difference between the total energy of the tetramer and the energy of a single molecule. The values, corrected by the basis set superposition error (BSSE) by the Boys and Bernardi counterpoise method [54], are reported in Table 1 and they show that PhOH and CycOH are more strongly bonded each other in the mixed tetramer with respect to the homotetramers. However it is worth observing that although hydrogen bonding is unequivocally the most relevant intermolecular interaction in pure as well as in mixed components, weaker van der Waals interactions could significantly contribute to the stability of the systems and the energy interaction values here reported take all the components into account in full. For a better characterization of the different interactions that really contribute to the stability of the tetramers we applied the NCI approach [55]. The NCI method, also known as reduced density gradient (RDG) method, is a valuable tool for studying and distinguishing van der Waals, hydrogen bonding, and steric repulsion interactions in the complexes [55]. The RDG isosurfaces for the tetramers are illustrated in Fig. 3 and interpreted through simple color codes [33]: the blue regions indicate highly attractive interactions, such as hydrogen bond, green regions indicate weak interactions, such as van der Waals contribution, and red regions indicate strong repulsion. In the case of the PhOH tetramer (Fig. 1a), intermolecular association is characterized by a localized interaction spot in the OH···O region corresponding to the hydrogen bond (blue color) and by spots (green regions) of limited extension corresponding to van der Waals interactions through hydrogen atoms of benzene ring and oxygen of the OH group. If the benzene rings are aligned to favor π-π interaction as in PhOH tetramer of Fig. 1,b, a massive van der Waals region between two rings is observed (Fig. S3) and this interaction is responsible of the higher stability of this tetramer, as observed above. For the CycOH tetramer in Fig. 3, along with the hydrogen bond spots, we observe green spots on an extended region corresponding to the stabilizing interaction between cyclohexyl rings. In the PhOH-CycOH tetramer in Fig. 3 we observe again hydrogen bond between molecules with spots more prominent in the OH···O region where phenol acts as HB donor, in agreement with that expected, and green spot surfaces of quite limited area suggesting that the interactions between benzene and cyclohexyl rings are weaker than that between cyclohexyl rings in the CycOH tetramer. The AIM analysis combined with the NCI study indicates therefore that heteroassociation is energetically preferred with respect to homoassociation in the PhOH-CycOH system because hydrogen bond is stronger between different components, however van der Waals interactions between cyclohexyl rings have a significant role in self association of cyclohexanol beyond the localized hydrogen bond.

To compare the features of our PhOH-CycOH binary system with that of the thymol-menthol mixture, we proposed the tetramers of thymol (Thym), menthol (Menth) and thymol-menthol (Thym-Menth) reproduced in Fig. S1 as models to study homoassociation and heteroassociation. We studied these oligomers by considering the same cyclic structures investigated for PhOH and CycOH to obtain their molecular properties at the same level of theory applied for the PhOH-CycOH system. Table 1 shows the hydrogen bond distances and the results of the topological analysis along with the energy interaction values, ΔE, obtained for each tetramer. All the results indicate that hydrogen bond between thymol and menthol is stronger than that between menthol and menthol and between thymol and thymol for the coupling of a good HB donor like thymol and a good HB acceptor like menthol. The effect is however less marked than that observed for the PhOH-CycOH system probably because phenol is slightly more acidic (pKa = 9.99)[56] than thymol (pKa = 10.62) [57]. A recent study on some thymol and menthol dimers confirmed the preferred tendency to heteroassociation of the Menth-Thym system [58]. This result is therefore substantially in agreement with our PhOH-CycOH system and, in particular, with the feature of hydrogen bond, however

**Table 1**
Hydrogen bond geometry (Å), topological analysis (a.u.) and interaction energy ΔE (kJ/mol) obtained at the M062X/6-311G** level for the tetramer models.

| | PhOH(Fig. 1a) | PhOH(Fig. 1b) | CycOH | PhOH + CycOH[a] |
|---|---|---|---|---|
| ρ ($r_c$) (a.u.) | 0.0372 | 0.0356 | 0.0411 | 0.0494 |
| $\nabla^2(r_c)$ (a.u.) | 0.1346 | 0.1277 | 0.138 | 0.1467 |
| $H(r_c)$ (a.u.) | −0.0007 | +0.0003 | −0.0022 | −0.0064 |
| *r*O···H (Å) | 1.756 | 1.788 | 1.738 | 1.665 |
| ΔE(kJ/mol) | −71 | −79 | −77 | −82 |
| | Thym(Fig. S1a) | Thym(Fig. S1b) | Menth | Thym + Menth[b] |
| ρ ($r_c$) (a.u.) | 0.0370 | 0.0316 | 0.0372/0.0381 | 0.0418 |
| $\nabla^2(r_c)$ (a.u.) | 0.1328 | 0.1183 | 0.1408/0.1305 | 0.1380 |
| $H(r_c)$ (a.u.) | −0.0007 | +0.0009 | −0.0014/-0.0023 | −0.0037 |
| *r*O···H (Å) | 1.762 | 1.832 | 1.792/1.778 | 1.749 |
| ΔE(kJ/mol) | -81 | −92 | −84 | −96 |

[a] Only PhOH. . .O values are reported
[b] Only ThymOH. . .O values are reported

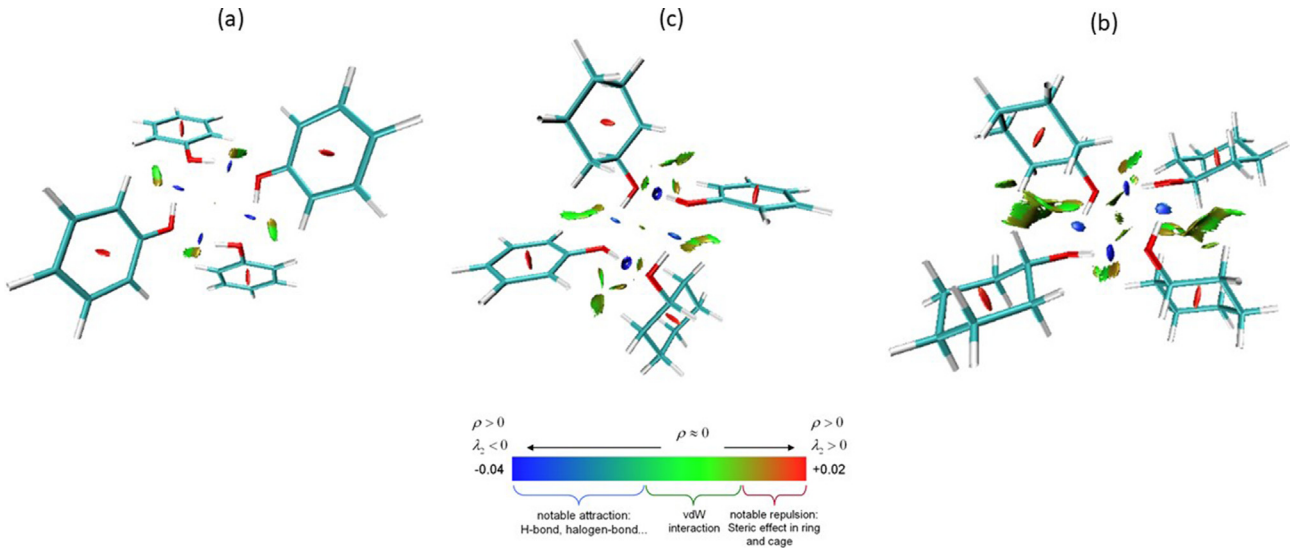


**Fig. 3.** NCI analysis for the PhOH, CycOH and PhOH-CycOH tetramers.

the alkyl groups present in the menthol and thymol molecules can play an additional and important stabilizing effect on the oligomers that is missing in the unsubstituted rings of phenol and cyclohexanol. The energy interaction values are in fact higher in all the Thym and Menth tetramers, as reported in Table 1. The role of the van der Waals interactions in this clusters is shown in Fig. S4 where the RDS isosurfaces are reported for each tetramer. It is interesting to observe that for the Thym-Menth tetramer NCI shows a van der Waals region between the alkyl chains more massive than that observed for the Menth-Menth tetramer suggesting that the more extensive interactions between alkyl chains along with a stronger hydrogen bond are the main causes that give higher stability to the thymol-menthol heteroassociation. Self association of thymol can be driven also by additional π-π interaction between benzene ring; as for phenol, geometry optimizations of the cyclic tetramer within the $S_4$ symmetry gives in fact a second structure (Fig. S3b) where the benzene rings are oriented to interact each other through their π electron density. Notwithstanding this further interaction between thymol molecules, clearly shown in the RDS isosurfaces reported in Fig. S3, the Thym-Menth tetramer is anyway the most stable structure with the highest energy interaction (Table 1).

### 3.3. Vibrational spectra

Infrared spectra of PhOH and CycOH are discussed in this section with the aim to find experimental evidence that reveals the role of the interactions between the components in the mixture. In particular, our aim is to investigate if the vibrational spectra of each component change upon mixing and try to correlate the spectral changes with the extent of the interactions between components. With this aim, we preliminarly compare each other the vibrational spectra calculated for the PhOH, CycOH and PhOH-CycOH tetramers and here reproduced in Fig. 4. The assignment of the main bands, based on the analysis of the normal modes, is reported in Fig. 4: in the spectrum of the PhOH-CycOH complex we have marked the bands assigned to each component with different colors. In the high frequency region, the OH stretching modes (ν) are indeed affected by the coordination pattern between components. Upon heteroassociation, the νOH frequencies move from their values calculated for the PhOH and CycOH homotetramers: in particular the ν mode of PhOH, acting as hydrogen bonding donor, shifts to lower frequency whereas the ν mode of CycOH, acting as hydrogen bonded acceptor, moves to higher frequency. These spectral pattern is fully consistent with the fact that hydrogen bonding between components strengthens by mixing and the frequency shifts of the νOH mode could be therefore diagnostic to indicate changes in the strength of the intermolecular interaction. Moreover the remaining vibrational modes of the OH group, the in plane (δ) and the out of plane (γ) bending, show frequency values again sensitive to the strength of the O(H)···O interaction. When different components are mixed, the δOH frequency of PhOH increases whereas the δOH frequency of CycOH decreases in agreement with the formation of a stronger hydrogen bond; the same and even more pronounced effect is expected for the γOH modes.

Following the results obtained from the theoretical spectra, we analyzed hydrogen bonds between different components on the basis of the spectral changes measured in the infrared spectra after mixing. We compare in Fig. 5 the experimental IR spectra of PhOH and CycOH pure components with the spectrum of liquid mixture at the $x_c$ = 0.85 composition. Assignment of the main bands, reported in Fig. 5, is based on the information from our calculated spectra and from literature for CycOH [59,60,43] and PhOH [61,62]. The OH stretching absorptions are very large in the spectra of the pure components and the frequency maximum is observed at about 3364 $cm^{-1}$ for PhOH and 3328 $cm^{-1}$ for CycOH. This band is slightly broader in the mixture than in the pure component spectra and this could suggest a slight variation in the coordination of the OH group. Due to the difficulty to assign the overlapping νOH bands of each component in the mixture spectrum, the absorption band was deconvoluted into two Gaussian-shape components [63] (Figure S5). The band profile is reproduced by two Gaussian components with maxima at 3254 $cm^{-1}$ and 3396 $cm^{-1}$, suggesting a small change in the vibration stretching frequency of the OH groups. In the medium frequency region, the δOH absorption of phenol appears as a shoulder of the more intense νCO band in the spectrum of pure phenol as well as in the spectrum of mixture; the δOH absorption of cyclohexanol is well distinguishable when the component is pure and when it is mixed and its frequency is substantially unchanged. The spectra continue to be very similar in the low frequency region where the γOH frequency of cyclohexanol seems to be quite unsensitive to the mixing whereas a small blue shift is measured for the γOH frequency of phenol. The infrared spectra show therefore that most absorptions of PhOH and CycOH in the mixture at eutectic composition are measured at fre-

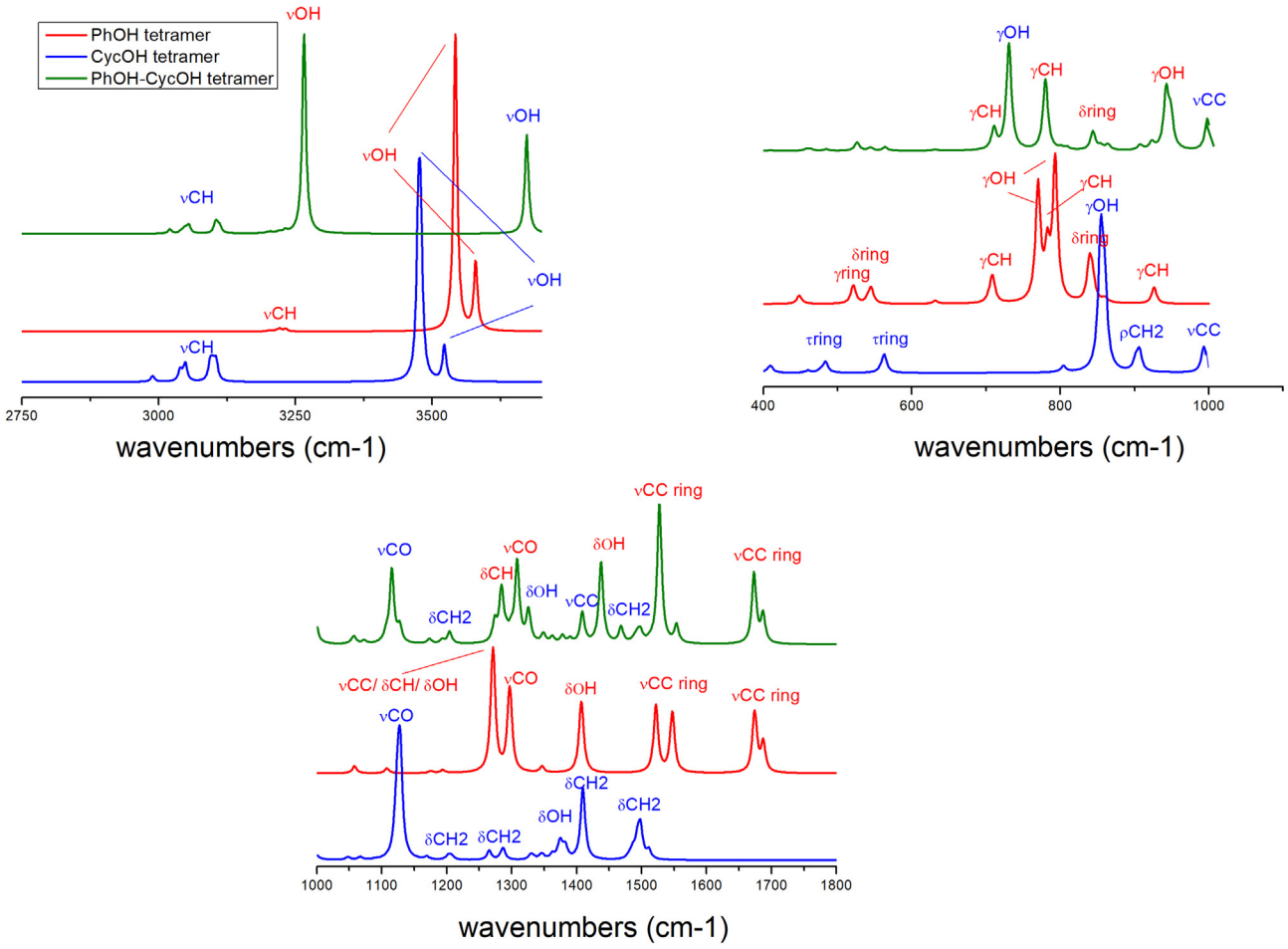


**Fig. 4.** Infrared spectra calculated at the M062X/6-311G** level for the tetramers of PhOH (Structure 1a), CycOH (Structure 1c) and PhOH-CycOH (Structure 1d).

quencies indeed close to that of the pure components. One can observe only small frequency blue shifts of the δOH and γOH vibrations of phenol that are in a qualitative agreement with the spectral features of the tetramers discussed above. The salient conclusion from the infrared analysis is that deviations from ideal mixing seem to be very small for our system, as already observed from DSC measurements.

We are aware that the interaction models studied so far are suitable for investigating the features of the intermolecular interactions between phenol and cyclohexanol and highlighting their differences: however they are 1:1 complexes that do not fully describe the interactions between components at the eutectic composition, where cyclohexanol is definitely more abundant. Therefore the morphology of the system at the eutectic composition has been investigated through molecular dynamics.

### 3.4. MD simulations

Since the GAFF force field covers almost all the organic species giving quite good results with various liquid systems [64–67] without the need for further parametrization, we decided to simulate our mixture using this force field and its structure was analyzed by monitoring firstly the hydrogen bond distances. Self association of PhOH and CycOH, described through the Radial Distribution Functions (RDFs) of the O···O contacts (Fig. 6a), reveals that interactions between cyclohexanol molecules, the most abundant component, clearly prevail on those between phenol molecules and, moreover, the relative peak is sharper and is observed at shorter distance. This is consistent with the fact that hydrogen bond between CycOH molecules is stronger than that between PhOH molecules, in agreement with the geometries of the tetramers discussed in the previous section. The presence of hydrogen bond between different components is clearly witnessed by the $O_{CycOH}\cdots O_{PhOH}$ peak at distances quite close to that of the $O_{CycOH}\cdots O_{CycOH}$ peak. The nature of the $O_{CycOH}\cdots O_{PhOH}$ intermolecular contact is revealed by the RDFs of the H···O distance of Fig. 6b: the peak of the $OH_{PhOH}\cdots O_{CycOH}$ distance is sharper and more intense than that of the $OH_{CycOH}\cdots O_{PhOH}$ one, consistently with the fact that the oxygen of PhOH acts as a better hydrogen bond donor, as already observed from the geometry of the mixed tetramer of Fig. 1. Distribution of the components in the mixture and the relative orientation of the rings of CycOH and PhOH can be studied by the RDFs of their center of mass positions. From Fig. 6c we observe that the CycOH-CycOH peak is quite symmetric and centred at about 6 Å; the PhOH-PhOH and CycOH-PhOH peaks show a maximum at very similar distances with a shoulder at lower values (about 5 Å). This slight asymmetry of the peak could be originated by the fact that PhOH, a planar molecule, could approach CycOH more closely than CycOH. Spatial Distribution Functions (SDF) of the center of mass of CycOH and PhOH around the cyclohexanol molecule (Fig. S6) shows that CycOH is distributed quite symmetrically whereas the small number of PhOH molecules in the mixture is oriented mainly around the OH group. The low concentration of phenol in the mixture at the eutectic composition and the absence of peaks at about 4 Å in the centre of mass RDFs seems exclude any π-π interaction between the benzene rings.

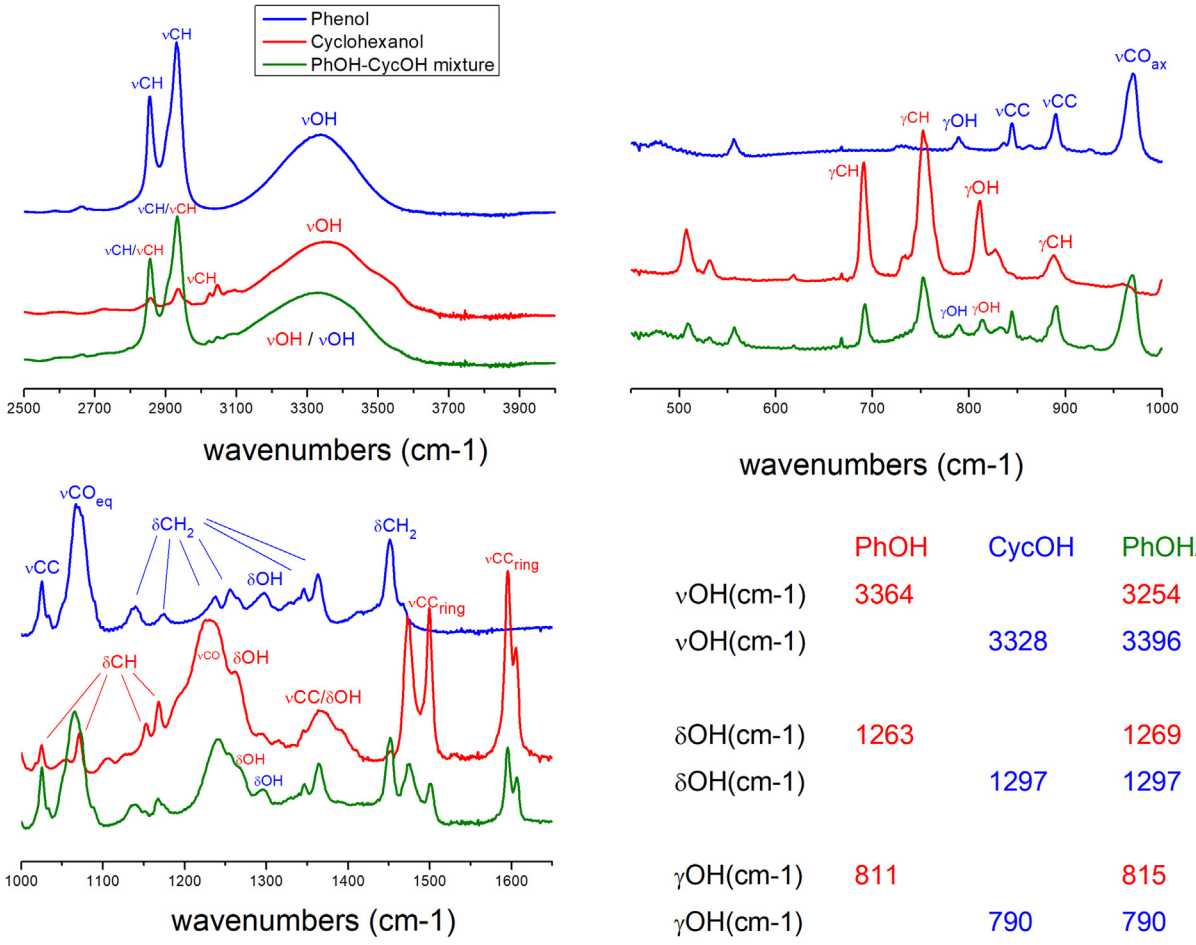


| | PhOH | CycOH | PhOH/CycOH |
|---|---|---|---|
| νOH(cm-1) | 3364 | | 3254 |
| νOH(cm-1) | | 3328 | 3396 |
| δOH(cm-1) | 1263 | | 1269 |
| δOH(cm-1) | | 1297 | 1297 |
| γOH(cm-1) | 811 | | 815 |
| γOH(cm-1) | | 790 | 790 |

**Fig. 5.** Infrared spectra measured for PhOH (red), CycOH (blue) pure components and the PhOH-CycOH at eutectic composition $x_c$ = 0.85 (green).

Homoassociations and heteroassociations have been also analyzed by calculating the number of H-bonds classified as medium on the basis of the geometrical criterium [68] (an HBD-HBA distance $\leqslant$3 Å and a D-H-A angle 30°) and the results are summarized in Table S2. At the eutectic composition, the number of PhOH-PhOH H-bonds is negligible whereas the distribution between PhOH-CycOH and CycOH-CycOH interactions is largely dominated by self association of cyclohexanol (about 80%). In addition, as observed from RDF analysis, the highest number of hydrogen bonds between PhOH-CycOH are found when phenol acts as the HBD and cyclohexanol as the HBA.

### 3.5. X-ray scattering

The structure of the mixture at the eutectic composition has been studied experimentally through X-ray diffraction and in Fig. 7 we report the X-ray structure function. A validation of the structural considerations derived from MD simulations and discussed above can be obtained by comparing the findings from the MD simulation with the measured X-ray diffraction pattern as shown in Fig. 7. The curve is dominated by the main peak at about 1.4 Å$^{-1}$ which correlates with distances at about 5 Å due to several intermolecular terms that mainly involve the C···C contributions. This value is consistent with the distance observed for the peaks of the RDFs of the center of mass positions discussed above. The experimental curve shows a second, much weaker and larger peak at about 3.2 Å$^{-1}$ that correlates with distances at about 2 Å in the direct space due to intramolecular contacts. The pattern above 5 Å$^{-1}$ corresponds again to intramolecular distances and is satisfactorily reproduced by our MD simulations. Good agreement is found for the main peak due to the intermolecular contributions (1.4 Å$^{-1}$) and for the remaining pattern whereas the X-ray diffraction curve at low $q$ value is reproduced with less accuracy. The X-ray curve shows also a small prepeak at about 0.5 Å$^{-1}$ that is barely noticeable in theoretical simulation. The existence of a prepeak located at $q$ values lower than 1 Å$^{-1}$ has been interpreted as evidence of a medium-range order due to the presence of heterogeneities or clustering phenomena induced by hydrogen bonding [69,70]. This effect has been observed in 1:1 Thym-Menth mixtures where the rings of menthol and thymol prevent the formation of a long network of hydrogen bond and allows the aggregation of molecules in small hydrogen bonded clusters [27]. Moreover the formation of oligomers consisting of thymol, menthol or thymol-menthol molecules are highly probable in the liquid at equimolar composition [27]. In our PhOH-CycOH mixture the X-ray diffraction has been measured at the eutectic composition where cyclohexanol is in a large excess and its ring has not alkyl substituent that could favor clustering phenomena. The prepeak in the X-ray curve is observed at a $q$ value, 0.55 Å$^{-1}$, that corresponds approximately to a distance (=2π/0.55 Å$^{-1}$) of about 11 Å. This intermolecular separation seems to be compatible with a distance C···C between carbon atoms of cyclohexanol rings oriented as reproduced in Fig. 1. In addition, this structural distribution of cyclohexanol molecules is in agreement with the RDFs of their center of mass positions that shows a second peak at about 11 Å.

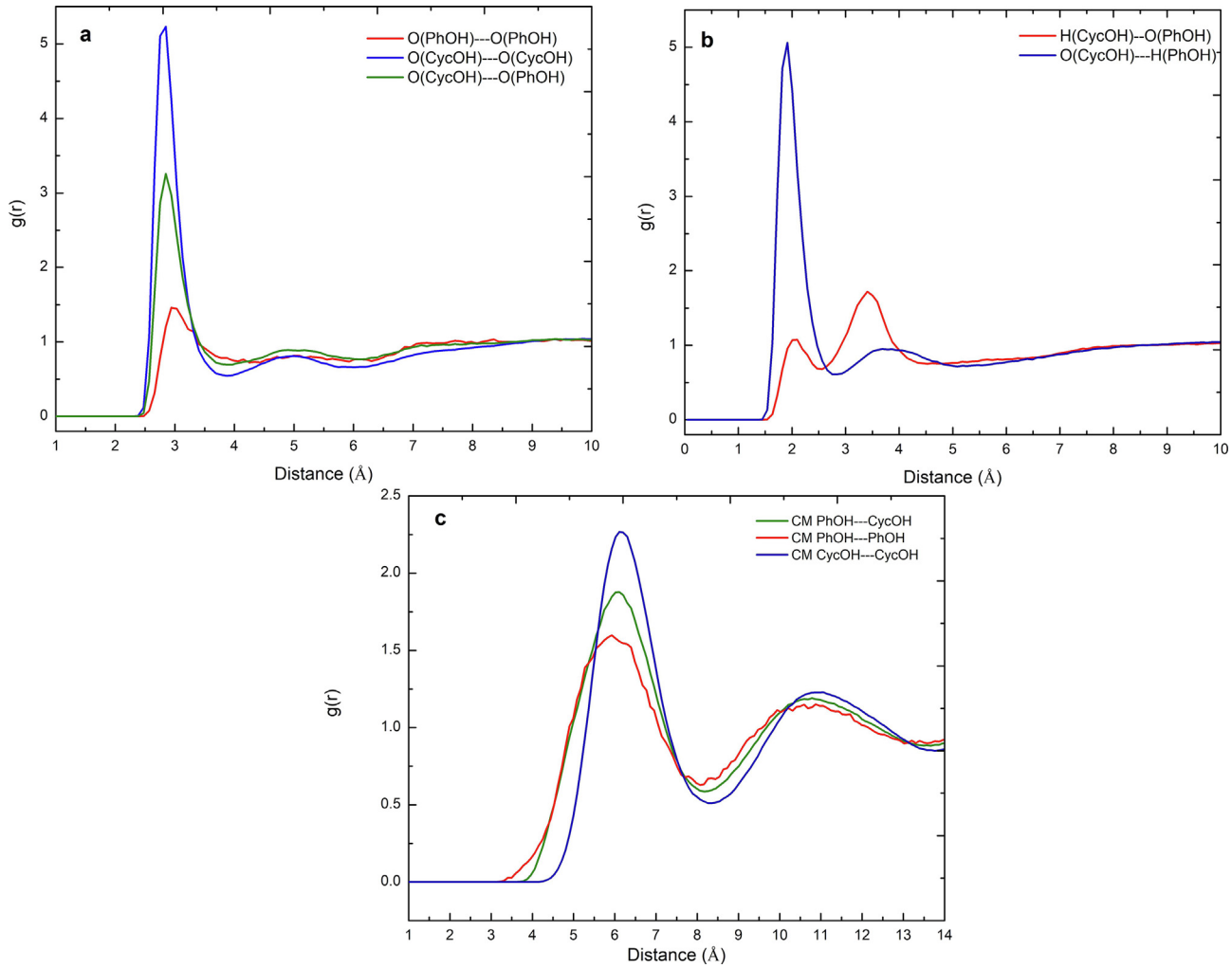


**Fig. 6.** RDFs of the O…O (a) and OH…O (b) distances and RDFs of the centre of mass positions (c).

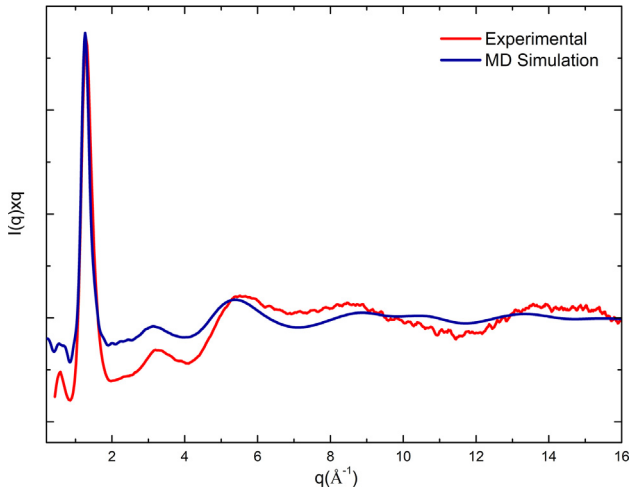


**Fig. 7.** Experimental and theoretical $I(q)q$ curves of the PhOH-CycOH mixture at eutectic composition.

## 4. Conclusions

The phenol-cyclohexanol mixtures have been studied using a combined experimental and theoretical approach. The SLE phase diagram, measured by DSC experiments, shows that the mixture at the eutectic composition ($x_c$) has melting point ($-35$ °$C$) strongly lower than pure components (25 °$C$ for cyclohexanol and 45 °$C$ for phenol). The extent of non ideality of the mixture has been evaluated in terms of interaction energies among the components by DFT methods. Self association and heteroassociation have been compared by calculations on some cyclic tetramers where phenol and cyclohexanol are linked by hydrogen bonds both like HB donor and HB acceptor. Intermolecular geometries, interaction energies and electron density properties indicate that intermolecular H-bond between different components is preferred with respect to homoassociation. Heteroassociation is favored also between thymol and menthol, a couple of molecules structurally very similar to phenol and cyclohexanol, and this preference has been identified as the main cause to explain the severe negative deviations from ideality observed for the Thym-Menth mixture. PhOH and CycOH seem therefore to be reliable precursors to form a DES [71], as for the Thym-Menth couple. In both systems the excellent HB donor property of the phenolic group coupled with the optimal HB acceptor property of the alcoholic OH group allow the formation of HB interactions that are stronger when components are mixed than those in the neat compounds. However our PhOH-CycOH mixtures show deviations from the ideal mixing much less pronounced than those observed for the Thym-Menth system, as suggested also from the IR spectra that, measured before and after mixing, showed quite unchanged bands. Notwith-

standing the similar chemical nature of the two systems, the observed discrepancies can be rationalized as follows. The eutectic composition of the thymol-menthol system is very close to an equimolar ratio where the number of Thym-Menth hydrogen bonds is maximum and the competing nature of the stronger Thym-Menth interaction results in a whole stabilization of the mixture and consequent negative deviation from ideality. The eutectic composition of the analogous PhOH-CycOH mixture is instead observed in presence of a strong excess of cyclohexanol, at a composition where the CycOH-CycOH interactions are dominant: the small number of more favourable PhOH-CycOH hydrogen bonds produces therefore a slight stabilizing effect on the mixture. Deviations from ideality are in fact expected more outstanding at equimolar composition. In addition, the NCI analysis indicates that heteroassociation and homoassociation of thymol and menthol molecules shows a nature not completely equivalent to that of our molecules for the presence of additional van der Waals contributions involving alkyl chains that are missing in PhOH and CycOH. The morphology of the mixture obtained by the analysis of the MD results confirm that the components of our mixture interact mainly via hydrogen bonding and the structural features observed in the X-ray diffraction experiments are substantially reproduced by the chosen potential of our MD simulations.

## Declaration of Competing Interest

The authors declare that they have no known competing financial interests or personal relationships that could have appeared to influence the work reported in this paper.

## Appendix A. Supplementary material

Supplementary data associated with this article can be found, in the online version, at https://doi.org/10.1016/j.molliq.2022.119492.

## References


[1] B.B. Hansen, S. Spittle, B. Chen, D. Poe, Y. Zhang, J.M. Klein, A. Horton, L. Adhikari, T. Zelovich, B.W. Doherty, B. Gurkan, E.J. Maginn, A. Ragauskas, M. Dadmun, T.A. Zawodzinski, G.A. Baker, M.E. Tuckerman, R.F. Savinell, J.R. Sangoro, Deep eutectic solvents: A review of fundamentals and applications, Chem. Rev. 121 (3) (2021) 1232–1285.

[2] Q. Zhang, K. De Oliveira Vigier, S. Royer, F. Jerome, Deep eutectic solvents: syntheses, properties and applications, Chem. Soc. Rev. 41 (2012) 7108–7146.

[3] E.L. Smith, A.P. Abbott, K.S. Ryder, Deep eutectic solvents (DESs) and their application, Chem. Rev. 114 (2014) 11060–11082.

[4] T.E. Achkar, H. Greige-Gerges, S. Fourmentin, Understanding the basics and properties of deep eutectic solvents: a review, Environmen, Chem. Lett. 19 (2021) 3397–3408.

[5] A. Mannu, M. Blangetti, S. Baldino, C. Prandi, Promising technological and industrial applications of deep eutectic systems, Materials (2021) 2494–2520.

[6] D.V. Wagle, H. Zhao, G.A. Baker, Deep eutectic solvents: Sustainable media for nanoscale and functional materials, Acc. Chem. Res. 47 (8) (2014) 2299–2308.

[7] M. Atilhan, S. Aparicio, Review and perspectives for effective solutions to grand challenges of energy and fuels technologies via novel deep eutectic solvents, Energy Fuels 35 (2021) 6402–6419.

[8] M. Zhou, O. Fakayode, A.A. Yagoub, Q. Ji, C. Zhou, Lignin fractionation from lignocellulosic biomass using deep eutectic solvents and its valorization, Renew. Sustain. 156 (2022) 111986–112000.

[9] O. Hammond, A.-V. Mudring, Ionic liquids and deep eutectics as a transformative platform for the synthesis of nanomaterials, Chem. Commun. 58 (2022) 3865–3892.

[10] M.A.R. Martins, S.P. Pinho, J.A.P. Coutinho, Insights into the nature of eutectic and deep eutectic mixtures, J. Solution Chem. 48 (2019) 962–982.

[11] S.L. Perkins, P.C. Painter, C.M. Colina, Experimental and computational studies of choline chloride-based deep eutectic solvents, J. Chem. Eng. Data 59 (2014) 3652–3662.

[12] O.S. Hammond, D.T. Bowron, K.J. Edler, Liquid structure of the choline chloride-urea deep eutectic solvent (reline) from neutron diffraction and atomistic modelling, Green Chem. 18 (2016) 2736–2744.

[13] L. Gontrani, M. Bonomo, N.V. Plechkova, D. Dini, R. Caminiti, X-ray structure and ionic conductivity studies of anhydrous and hydrated choline chloride and oxalic acid deep eutectic solvents, Phys. Chem. Chem. Phys. 20 (2018) 30120–30124.

[14] C. Florindo, F.S. Oliveira, L.P.N. Rebelo, A.M. Fernandes, I.M. Marrucho, Insights into the synthesis and properties of deep eutectic solvents based on cholinium chloride and carboxylic acids, ACS Sustain. Chem. Eng 2 (10) (2014) 2416–2425.

[15] A.K. Dwamena, Recent advances in hydrophobic deep eutectic solvents for extraction, Separations 6 (2019) 9–24.

[16] D. van Osch, C. Dietz, S. Warrag, M. Kroon, The curious case of hydrophobic deep eutectic solvents: a story on the discovery, design, and applications, ACS Sustain. Chem. Eng. 8 (2020) 10591–10612.

[17] D.J. van Osch, L.F. Zubeir, A. van den Bruinhorst, M.A. Rochaa, M.C. Kroon, Hydrophobic deep eutectic solvents: Water-immiscible extractants, Green Chem. 17 (2015) 4518–4521.

[18] L. Zubeir, D.V. Osch, M. Rocha, F. Banat, M. Kroon, Carbon dioxide solubilities in decanoic acid-based hydrophobic deep eutectic solvents, J. Chem. Eng. Data 63 (2018) 913–919.

[19] M. Usanovich, On the deviations from the Raoult's law due to chemical interactions between the components, Dok. Acad. Nauk. SSSR 120 (1958) 1304–1306.

[20] S. Suriyanarayanan, G.D. Olsson, S. Kathiravan, N. Ndizeye, I.A. Nicholls, Non-ionic deep eutectic liquids: Acetamide-urea derived room temperatures solvents, Int. J. Mol. Sci. 20 (2019) 2857–2867.

[21] N. Ndizeye, S. Suriyanarayanan, I.A. Nicholls, Polymer synthesis in non-ionic deep eutectic solvents, Polym. Chem. 10 (2019) 5289–5295.

[22] Y. Cui, J.C. Rushing, S. Seifert, N.M. Bedford, D.G. Kuroda, Molecularly heterogeneous structure of a nonionic deep eutectic solvent composed of n-methylacetamide and lauric acid, J. Phys. Chem. B 123 (2019) 3984–3993.

[23] H.P. Urvi Gala, H. Chauhan, Pharmaceutical applications of eutectic mixtures, J. Dev. Drugs 2 (2013) 1–26.

[24] M.A.R. Martins, E.A. Crespo, P.V.A. Pontes, L.P. Silva, M. Bülow, G.J. Maximo, E.A. C. Batista, C. Held, S.P. Pinho, J.A.P. Coutinho, Tunable hydrophobic eutectic solvents based on terpenes and monocarboxylic acids, ACS Sustain. Chem. Eng. 6 (2018) 8836–8846.

[25] M.A.R. Martins, L.P. Silva, N. Schaeffer, D.O. Abranches, G.J. Maximo, S.P. Pinho, J.A.P. Coutinho, Greener terpene–terpene eutectic mixtures as hydrophobic solvents, ACS Sustain. Chem. Eng. 7 (2019) 17414–17423.

[26] D.O. Abranches, M.A.R. Martins, L.P. Silva, N. Schaeffer, S.P. Pinho, J.A.P. Coutinho, Phenolic hydrogen bond donors in the formation of non-ionic deep eutectic solvents: the quest for type V des, Chem. Commun. 55 (2019) 10253–10256.

[27] N. Schaeffer, D.O. Abranches, L.P. Silva, M.A. Martins, P.J. Carvalho, O. Russina, A. Triolo, L. Paccou, Y. Guinet, A. Hedoux, J.A. Coutinho, Non-ideality in thymol + menthol type V deep eutectic solvents, ACS Sustain. Chem. Eng. 9 (2021) 2203–2215.

[28] D.K. Panda, B. Bhargava, Molecular dynamics investigation of non-ionic deep eutectic solvents, J. Mol. Graph. Model. 113 (2022) 108152–108160.

[29] M.J. Frisch, G.W. Trucks, H.B. Schlegel, G.E. Scuseria, M.A. Robb, J.R. Cheeseman, G. Scalmani, V. Barone, B. Mennucci, G.A. Petersson, et al., Gaussian 09, Revision C.01, Gaussian Inc., Wallingford CT, 2010.

[30] Y. Zhao, D. Truhlar, The M06 suite of density functionals for main group thermochemistry, thermochemical kinetics, noncovalent interactions, excited states, and transition elements: two new functionals and systematic testing of four M06-class functionals and 12 other functionals, Theor. Chem. Acc. 120 (2008) 215–241.

[31] D.V. Wagle, C. Deakyne, G. Baker, Quantum chemical insight into the interactions and thermodynamics present in choline chloride based deep eutectic solvents, J. Phys. Chem. B 120 (2016) 6739–6746.

[32] A.K. Todd, AIMAll (Version 19.10.12), TK Gristmill Software, Overland Park KS, USA, 201, 2010.

[33] T. Lu, F. Chen, Multiwfn: A multifunctional wavefunction analyzer, J. Comput. Chem. 33 (2012) 580–592.

[34] J. Wang, R. Wolf, J. Caldwell, P. Kollman, D. Case, Development and testing of a general amber force field, J. Comput. Chem. 25 (2004) 1157–1174.

[35] D. Case, I. Ben-Shalom, S. Brozell, D. Cerutti, T.C. III, V. Cruzeiro, T. Darden, R. Duke, D. Ghoreishi, M. Gilson, H. Gohlke, A. Goetz, D. Greene, R. Harris, N. Homeyer, S. Izadi, A. Kovalenko, T. Kurtzman, T. Lee, S. LeGrand, P. Li, C. Lin, J. Liu, T. Luchko, R. Luo, D. Mermelstein, K. Merz, Y. Miao, G. Monard, C. Nguyen, H. Nguyen, I. Omelyan, A. Onufriev, F. Pan, R. Qi, D. Roe, A. Roitberg, C. Sagui, S. Schott-Verdugo, J. Shen, C. Simmerling, J. Smith, R. Salomon-Ferrer, J. Swails, R. Walker, J. Wang, H. Wei, R. Wolf, X. Wu, L. Xiao, D. York, P. Kollman, Amber 18, Amber 2018, University of California, San Francisco, 2018.

[36] F. Dupradeau, A. Pigache, T. Zaffran, C. Savineau, R. Lelong, N. Grivel, D. Lelong, W. Rosanski, P. Cieplak, The r.e.d. tools: advances in resp and esp charge derivation and force field library building, Phys. Chem. Chem. Phys. 12 (2010) 7821–7839.

[37] B. Hess, H. Bekker, H.J.C. Berendsen, J.G.E.M. Fraajie, Lincs: A linear constraint solver for molecular simulations, J. Comput. Chem. 18 (1997) 1463–1472.

[38] L. Martinez, R. Antrade, E.G. Birgin, J.M. Martinez, Packmol: A package for building initial configurations for molecular dynamics simulations, J. Comput. Chem. 30 (2009) 2157–2164.

[39] M. Brehm, B. Kirchner, Travis - a free analyzer and visualizer for monte carlo and molecular dynamics trajectories, J. Chem. Inf. Model 51 (2011) 2007–2023.

[40] O. Holloczki, M. Macchiagodena, H. Weber, M. Thomas, M. Brehm, A. Stark, O. Russina, A. Triolo, B. Kirchner, Triphilic ionic-liquid mixtures: Fluorinated and

non-fluorinated aprotic ionic-liquid mixtures, ChemPhysChem 16 (2015) 3325–3333.
[41] E.J.R., L.C.T., Introductory Chemical Engineering Thermodynamics, second ed., Upper Saddle River, NJ, Prentice Hall, 2012.
[42] J.R. Green, W.T. Griffith, Polymorphism in cyclohexanol reexamined, Mol. Cryst. Liq. Cryst. 6 (1969) 23–40.
[43] D.W. James, H.F. Shurvell, R.M. Parry, Polymorphism in cyclohexanol: A Raman spectroscopic study, J. Raman Spectr. 5 (1976) 201–209.
[44] R.M. Ibberson, S. Parsons, D.R. Allan, A.M.T. Bell, Polymorphism in cyclohexanol, Acta Cryst. B B 64 (2008) 573–582.
[45] L. Horng Jang, L. Shen-Chun, Binary mixtures exhibiting maximum flash-point behavior, J. Haz. Mat. 140 (2007) 155–164.
[46] D.R. Cova, Vapor-liquid equilibria in binary and ternary systems cyclohexanol-phenol, cyclohexanone-cyclohexanol, and cyclohexanol-phenol-cyclohexanone, J. Chem. Eng. Data 5 (1960) 282–284.
[47] V.E. Zavodnik, V.K. Belskii, P. Zorkii, Crystal structure of phenol at 123 K, J. Struct. Chem. 28 (1988) 175–177.
[48] F. Ramondo, L. Bencivenni, G. Portalone, A. Domenicano, Effect of intermolecular OH···O hydrogen bonding on the molecular structure of phenol: An ab initio molecular orbital study, Struct. Chem. 6 (1995) 37–45.
[49] M. Hartmann, M. Jenau, A. Wurflinger, M. Godlewska, S. Urban, High pressure DTA study on the phase behaviours in some selected plastic and liquid crystals, Z. Phys. Chem. 177 (1992) 195–210.
[50] O. Andersson, R. Ross, G. Backstrom, Thermal conductivity of crystalline and glassy crystal cyclohexanol under pressure, Mol. Phys. 66 (1989) 619–635.
[51] A. Lemmerer, C. Esterhuysen, OHphenol···OHalcohol hydrogen-bonding as the preferred hydrogen-bonded interaction in the crystal structures of three isomers of methylolphenol: analysis of hydrogen-bonding interactions in phenol and alcohol containing molecules, CrystEngComm 13 (2011) 5773–5782.
[52] U. Koch, P.L.A. Popelier, Characterization of C-H-O hydrogen bonds on the basis of the charge density, J. Phys. Chem. 99 (1995) 9747–9754.
[53] I. Rozas, I. Alkorta, J. Elguero, Behavior of ylides containing N, O, and C atoms as hydrogen bond acceptors, J. Am. Chem. Soc. 122 (2000) 11154–11161.
[54] S.F. Boys, F. Bernardi, The calculation of small molecular interactions by the differences of separate total energies. some procedures with reduced errors, Mol. Phys. 19 (1970) 553–566.
[55] E. Johnson, S. Keinan, P. Mori-Sanchez, J. Contreras-García, A. Cohen, W. Yang, Revealing noncovalent interactions, J. Am. Chem. Soc. 132 (2010) 6498–6506.
[56] E.P. Serjeant, B. Dempsey, CRC Handbook of Chemistry and Physics. 83rd IUPAC Chem Data Ser (2002-2003) 8–49.
[57] E.P. Serjeant, B. Dempsey, Ionisation constants of organic acids in aqueous solution, IUPAC Chem. Data Ser. 23 (1979) 989.
[58] A. Gutierrez, L. Zamora, C. Benito, M. Atilhan, S. Aparicio, Insights on novel type V deep eutectic solvents based on levulinic acid, J. Chem. Phys. 156 (2022) 94504–94523.
[59] M.A. Czarnecki, A.S. Muszynski, H. Troczynska, Molecular structure and hydrogen bonding in liquid cyclohexanol and cyclohexanol/water mixtures studied by FT-NIR spectroscopy and DFT calculations, J. Mol. Struct. 974 (2010) 60–67.
[60] L.M. Babkov, N.A. Davydova, E.A. Moisejkina, Hydrogen bonding and its influence on the structure and vibrational spectra of cyclohexanol, Izvestiya of Saratov University, New Series. Series Physics 13 (2013) 13–26.
[61] J.C. Evans, The vibrational spectra of phenol and phenol-OD, Spectroch. Acta 16 (1960) 1382–1392.
[62] D. Michalska, D.C. Bienko, A.J. Abkowicz-Bienko, Z. Latajka, Density functional, Hartree-Fock, and MP2 studies on the vibrational spectrum of phenol, J. Phys. Chem. 100 (1996) 17786–17790.
[63] M. Wojdyr, Fityk: a general-purpose peak fitting program, J. Appl. Cryst. 43 (2010) 1126–1128.
[64] L. Tanzi, F. Ramondo, R. Caminiti, M. Campetella, A. Di Luca, L. Gontrani, Structural studies on choline-carboxylate bio-ionic liquids by x-ray scattering and molecular dynamics, J. Chem. Phys. 143 (2015) 114506–114510.
[65] L. Tanzi, M. Nardone, P. Benassi, F. Ramondo, R. Caminiti, L. Gontrani, Choline salicylate ionic liquid by X-ray scattering, vibrational spectroscopy and molecular dynamics, J. Mol. Liq. 218 (2016) 39–49.
[66] S. Di Muzio, F. Ramondo, L. Gontrani, F. Ferella, M. Nardone, B.P., Choline hydrogen dicarboxylate ionic liquids by X-ray scattering, vibrational spectroscopy and molecular dynamics: H-fumarate and H-maleate and their conformations, Molecules 25 (2020) 4990–5009.
[67] S. Di Muzio, O. Russina, D. Mastrippolito, P. Benassi, L. Rossi, F. Ramondo, Mixtures of choline chloride and tetrabutylammonium bromide with imidazole as examples of deep eutectic solvents: their structure by theoretical and experimental investigation, J. Mol. Liq. 352 (2022) 118427–118436.
[68] G.R. Desiraju, T. Steiner, The weak hydrogen bond-in structural chemistry and biology, Oxford University Press, New York.
[69] O. Russina, A. Triolo, L. Gontrani, R. Caminiti, Mesoscopic structural heterogeneities in room-temperature ionic liquids, J. Phys. Chem. Lett. 3 (2011) 27–33.
[70] M. Campetella, F. Cappelluti, L. Gontrani, Medium range interactions evidences in compounds with aliphatic lateral chain: 1-pentanoic acid, 1-pentanol and pentylammonium nitrate as test cases, Chem. Phys. Lett. 734 (2019) 136738–136741.
[71] D. Abranches, J. Coutinho, Type V deep eutectic solvents: Design and applications, Current Opinion in Green and Sustainable Chemistry 48.